Supporting Information: A Synthetic Mimic of Phosphodiesterase Type 5 based on Corona Phase Molecular Recognition of Single-Walled Carbon Nanotubes

Juyao Dong, Michael A. Lee, Ananth Govind Rajan, Imon Rahaman, Jessica H. Sun, Minkyung Park, Daniel P. Salem, and Michael S. Strano*

Department of Chemical Engineering, Massachusetts Institute of Technology, 77 Massachusetts Avenue, Cambridge, Massachusetts 02139

E-mail: strano@mit.edu

Contents

www.pnas.org/cgi/doi/10.1073/pnas.1920352117

1 Experimental section

Materials

Styrene (contains 4-tert-butylcatechol as stabilizer, 99 %, Sigma-Aldrich), methacrylic acid (250 ppm MEHQ as inhibitor, 99 %, Sigma-Aldrich), inhibitor removers (replacement packing, for removing hydroquinone and monomethyl ether hydroquinone, Sigma-Aldrich), inhibitor removers (replacement packing, for removing tert-butylcatechol, Sigma-Aldrich), 4-cyano-[(dodecylsulfanylthiocarbonyl) sulfanyl]pentanoic acid, (97 %, Sigma-Aldrich), 2-2′-azobis(2-methylpropionitrile) (AIBN, recrystallized 99 %, Sigma-Aldrich), 1,4 dioxane (anhydrous, 99.8 %, Sigma-Aldrich), diethyl ether (99 %, Sigma-Aldrich), tetrahydrofuran (THF, 99.9 %, Sigma-Aldrich), phosphate buffered saline (PBS, 1×, without calcium and magnesium, Corning Cellgro), dimethyl sulfoxide (DMSO, 99.7 %, Sigma-Aldrich), sodium hydroxide (pellets, Macron Fine Chemicals), single-walled carbon nanotube (SWNTs, HiPCO), Vardenafil Hydrochloride (Sigma-Aldrich), Valacyclovir Hydrochloride (Sigma-Aldrich), Bupropion Hydrochloride (Sigma-Aldrich), Sumatriptan Succinate (99 %, solid, Sigma-Aldrich), Fluticasone Propionate (Sigma-Aldrich), 3-chlorostyrene (98 %, Sigma-Aldrich), 3-vinylphenyl boronic acid (95 %, Sigma-Aldrich), 4-chlorostyrene (97 %, Sigma-Aldrich), 4-vinylbenzoic acid (97 %, Sigma-Aldrich), 4-bromostyrene (97 %, Sigma-Aldrich), 3-bromostyrene (97 %, Sigma-Aldrich), maleimide (99 %, Sigma-Aldrich), L-threonine (98 %, Sigma-Aldrich), L-serine (99 %, Sigma-Aldrich), L-alanine (98 %, Sigma-Aldrich), L-lysine (98 %, Sigma-Aldrich), L-cysteine (97 %, Sigma-Aldrich), L-proline (99 %, Sigma-Aldrich), L-glycine (99 %, Sigma-Aldrich), PDE5A (OriGene Technologies), Tadalafil (98 %, HPLC, Sigma-Aldrich), Guanosine 3′, 5′-cyclic monophosphate (cGMP, 98 % HPLC, Sigma-Aldrich), Sildenafil (methanol solution, Sigma-Aldrich), acrylic acid (anhydrous, contains 200 ppm MEHQ as inhibitor, 99 %, Sigma-Aldrich), and PEG/PEO calibration kit (Agilent) were used without further modification.

Characterization

The ultracentrifugation was carried out using a Beckman Coutler with an SW32 Ti rotor. The absorption spectrum of the carbon nanotube solution was collected by a UV-vis-nIR spectrophotometer (Agilent Technologies, Cary 5000). The near-IR emission spectra were recorded by a home-built near-infrared fluorescence spectrometer. A Zeiss AxioVision inverted microscope was coupled with a nitrogen-cooled InGaAs detector (Princeton Instruments InGaAs OMA V) through a PI Acton SP2500 spectrometer. The nanotubes were excited by a 785 nm photodiode laser, 450 mW at the source and 150 mW at the sample plane. The 2D excitation-emission spectra are collected using the same InGaAs detector with a supercontinuum laser for the excitation (NKT Photonics). The particle size analysis was carried out by a dark-field scattering microscopy by Malvern Instruments Ltd. (NanoSight LM10) with a 405 nm laser. The exposure time for each collection was 30 s, and the results were averaged over 31 exposures. NMR spectra were collected by a Varian Inova 500 instrument (see the spectra for experimental parameters). Gel permeation chromatography (GPC) was carried out on a 1260 Infinity from Aglient Technologies. The plate reader used is a Microplate reader Varioscan Flash from Thermo Scientific.

Polymers synthesis and characterization

The amphiphilic polymers used to construct the corona phase were synthesized using reversible addition-fragmentation chain transfer (RAFT) polymerization, using AIBN as the initiator and appropriate RAFT agent. The MEHQ and 4-tert-butylcatechol were removed by passing through columns of inhibitor removers. Monomer ratios and their ratio against the RAFT agent and AIBN are tuned for different polymer compositions. For example, to synthesize the MA-ST-90 polymer for the screening, 373.4 mg of 4-cyano-4 [(dodecyl-sulfanylthiocarbonyl) sulfanyl]pentanoic acid (RAFT agent, 1 equiv.), 30.4 mg AIBN (0.5 equiv.), 1883 μl methacrylic acid (26 equiv.), and 638 μl styrene (4 equiv.) were dissolved in 10 ml dioxane. The reaction vial was purged with N_2 for 30 min before the reaction and the reaction was conducted at 68 °C for 24 hours under N_2 protection.

The polymers were purified through a series of precipitation and dissolution steps. First, the reaction solution was added dropwise into about 200 ml diethyl ether to precipitate out the polymer. Then, the precipitate was collected through filtration and dissolved in about 15 ml THF. The solution was precipitated in diethyl ether and the procedure was repeated three times. The polymer powder collected at the end was placed under vacuum for three days.

NMR spectra of polymer reaction mixtures were collected to calculate the conversion rate. NMR spectra of purified polymers were used to examine the polymer structure. For the conversion rate parte, approximately 50 μl of the reaction solution before and after polymerization were collected and dissolved in 650 μl deuterated methanol. For purified polymers, 50 mg of powder was dissolved in 700 μl DMSO. NMR spectra collected include ^{1}H and ^{13}C NMR along with 2D DQF-COSY and HSQC.

Gel permeation chromatography was used to analyze the distribution of molecular weights of polymers. 2 L of 0.2 M $NaNO_3$ and 0.01 M NaH_2PO_4 buffer solution was made and the pH was adjusted to neutral, as the mobile phase. Calibration standards were dissolved in this buffer solution at a concentration of 5 mg/ml. Purified polymers were dissolved in the same buffer solution and the pH was adjusted the neutral. The solution was filtered by a 0.5 μM filter before GPC test. All results are the average of triplets.

Polymer-SWNT suspension

20 mg of polymer (10 equiv.) was dissolved in 2 ml of water, with the addition of (1.5 M) sodium hydroxide solution to adjust pH. Approximately 2 mg HiPCO SWNT (1 equiv.) was added and the mixture was sonicated by a probe sonicator using a 6 mm probe tip at 10 W for 45 min. The resulting solution was ultracentrifuged at 35500 rpm for 4 h to remove the unsuspended or bundled particles. The collected supernatant solution was transferred into an Amicon filter device and centrifuged to remove any free polymers. Ultraviolet-visible-nIR absorption spectra and dark-field particle scattering microscopy were collected to characterize the polymer-SWNT suspensions.

Fluorescence spectrum collection

To collect the near IR emission spectra of polymer-SWNT suspensions. The as-prepared colloidal solutions were diluted to 1 mg/L, mixed with 2 vol % of drug analytes in DMSO or PBS solutions. The spectral control is made of similar aqueous solution with 2 vol % of DMSO or PBS without nanotubes. Fluticasone propionate, Sumatriptan succinate, Vardenafil hydrochloride, cGMP, Sildenafil and Tadalafil were dissolved in DMSO, while Bupropion hydrochloride and Valacyclovir hydrochloride were dissolved in PBS. Following incubation for 5 min on a tabletop shaker, the fluorescent spectra of the SWCNT were recorded using the home-built nIR fluorescence spectrometer.

Molecular dynamics simulations

Molecular dynamics (MD) simulations were carried out to determine the equilibrium polymeric corona phase configuration on the SWNT surface using the open-source GROMACS package (v4.6.5).[S2] The OPLS/AA force field[S3–S9] was utilized to model the polymer chains, which were built using the pdb2gmx command and suitable rtp entries for the monomeric units. Bond, angle and dihedral parameters that were not available in the original OPLS/AA

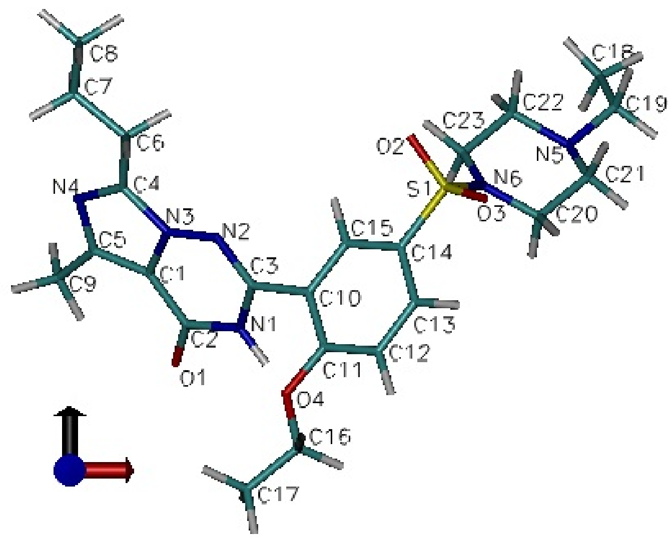

Figure S1: Structure of Vardenafil with the corresponding labeling of atoms.[S1]

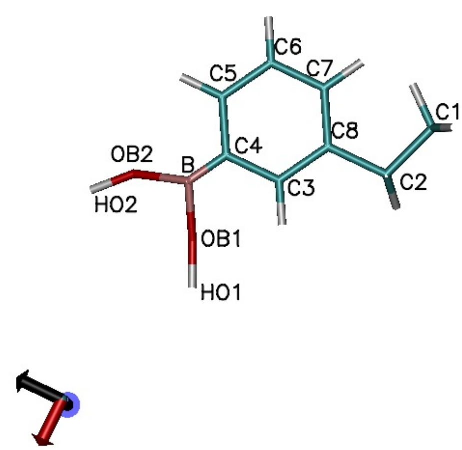

Figure S2: Structure of 3-phenylboronic acid in the polymer with corresponding labeling of atoms. B is boro_001; HO1 and HO2 are boro_002 (HOB); C4 is the boro_003 (CBO); OB1 and OB2 are boro_004 (OBO).

force field were modeled using parameters for similar structures included in other force field models, as listed in Table S1. Specifically, the parameters for phenylboronic acid and Vardenafil were adapted from the GROMOS 54A7 force field,[S10] generated using the Automated Topology Builder toolkit (listed in Table S1).[S1] The SWNTs and polymer chains were built using the Materials Studio (v8.0) software package and exported as PDB files before being converted into GRO files. A (6,5) SWNT of a unit-cell length was placed in the center of a simulation box of dimensions 8 nm × 8 nm × 4.06378 nm, with the polymer chain placed perpendicular to the SWNT at the center. The simulation box was filled with approximately 8400 water molecules (modeled using the TIP4P/2005 force field)[S11] and was periodic in all three directions. Counter ions (Na^+, 18 for MA-ST-90) were added to neutralize the electric charge. The simulation was started with an energy minimization loop for 50000 steps with an initial step-size of 0.01 nm. The energy minimization loop was followed by a 40 ns NVT ensemble run using a 2 fs time step. The system temperature was set to 300 K using the Bussi-Parinello thermostat.[S12] The NVT ensemble run was followed by a 30 ns NPT ensemble run, again using a 2 fs time step, leading to a total of 70 ns of simulation time. The system pressure was set to 1 bar using the Parrinello-Rahman barostat.[S13,S14] Lennard-Jones interactions were cutoff at a distance of 1.2 nm. Long-range electrostatic interactions were calculated using the Particle Mesh Ewald (PME) scheme.[S15] The position of the SWNT atoms were fixed. Bonds terminating in hydrogen atoms were constrained using the parallel version of the LINCS algorithm.[S16] The g_sas command was utilized to calculate the solvent accessible surface area. The g_msd command was utilized to calculate the mean square displacement of MA-ST polymer and Vardenafil. The g_dist command was utilized to calculate the center-of-mass distance between polymer and nanotube, and between Vardenafil and nanotube.

Table S1: Force-field parameters utilized in the MD simulations

atomtypes

	mass (a.m.u.)	atom
boro_001	10.811	B
boro_002	1.008	H

boro_003	12.011	C
boro_004	15.9994	O

aminoacids

Phenylboronic acid

	atom_type	charge (e)
C1	opls_136	-0.12
H13	opls_140	0.06
C2	opls_137	-0.06
H11	opls_140	0.06
H22	opls_140	0.06
C3	opls_145	-0.115
H3	opls_146	0.115
C4	boro_003	-0.14
B	boro_001	0.62
C5	opls_145	-0.115
H5	opls_146	0.115
C6	opls_145	-0.115
H6	opls_146	0.115
C7	opls_145	-0.115
H7	opls_146	0.115
C8	opls_145B	0
OB1	boro_004	-0.69
OB2	boro_004	-0.69
HO2	boro_002	0.45
HO1	boro_002	0.45

Styrene

	atom_type	charge (e)
C8	opls_145B	0
C3	opls_145	-0.115
H3	opls_146	0.115
C4	opls_145	-0.115
H4	opls_146	0.115
C5	opls_145	-0.115
H5	opls_146	0.115
C6	opls_145	-0.115
H6	opls_146	0.115
C7	opls_145	-0.115
H7	opls_146	0.115
C2	opls_137	-0.06
H22	opls_140	0.06
C1	opls_136	-0.12
H11	opls_140	0.06
H13	opls_140	0.06

Methacrylic acid

	atom_type	charge (e)
C1	opls_135	-0.12
HC3	opls_140	0.06
C2	opls_135	-0.1
C4	opls_271	0.7
O	opls_272	-0.8
O1	opls_272	-0.8
C3	opls_135	-0.18
H31	opls_140	0.06
H32	opls_140	0.06
H33	opls_140	0.06

Vardenafil

	atom_type	charge (e)
H19	opls_140	0.06
C17	opls_135	-0.18
H17	opls_140	0.06
H18	opls_140	0.06
C16	opls_136	0.14
H15	opls_140	0.03
H16	opls_140	0.03
O4	opls_182	-0.285
C11	opls_166	0.085
C12	opls_145	-0.115
H12	opls_146	0.115
C13	opls_145	-0.115
H13	opls_146	0.115
C10	opls_145	0.18
C15	opls_145	-0.115
H14	opls_146	0.115
C3	opls_642	0.965
N1	opls_641	-0.951
H1	opls_643	-0.014
C2	opls_280	0.47
O1	opls_281	-0.47
C1	opls_538	0.378
C5	opls_560	0.185
N4	opls_559	-0.563
C9	opls_674	-0.18
H9	opls_140	0.06
H10	opls_140	0.06
H11	opls_140	0.06
C4	opls_558	0.378
N3	opls_537	-0.331
N2	opls_537	-0.331
C6	opls_675	0.164
H2	opls_140	0.06
H3	opls_140	0.06
C7	opls_136	-0.12
H4	opls_140	0.06
H5	opls_140	0.06
C8	opls_135	-0.18
H6	opls_140	0.06
H7	opls_140	0.06
H8	opls_140	0.06
C14	opls_488	-0.12
S1	opls_474	1.48
O2	opls_475	-0.68
O3	opls_475	-0.68
N6	opls_478	-0.6
C20	opls_484	0.09
H25	opls_485	0.06
H26	opls_485	0.06
C21	opls_908	0.09

HC2	opls_140	0.06	H27	opls_911	0.06
			H28	opls_911	0.06
Acrylic acid			N5	opls_902	-0.63
C1	opls_135	-0.12	C23	opls_484	0.09
HC3	opls_140	0.06	H31	opls_485	0.06
C2	opls_135	-0.16	H32	opls_485	0.06
C4	opls_271	0.7	C22	opls_908	0.09
O	opls_272	-0.8	H29	opls_911	0.06
O1	opls_272	-0.8	H30	opls_911	0.06
HC2	opls_140	0.06	C19	opls_908	0.09
H12	opls_140	0.06	H23	opls_911	0.06
			H24	opls_911	0.06
			C18	opls_135	-0.18
			H20	opls_140	0.06
			H21	opls_140	0.06
			H22	opls_140	0.06

ffnonbonded

	name	charge (e)	sigma (nm)	epsilon (kJ/mol)
boro_001	B	0.62	0.358118	2.77E-01
boro_002	HOB	0.45	0	0.00E+00
boro_003	CBO	-0.14	0.352053	3.07E-01
boro_004	OBO	-0.69	0.340025	5.00E-01

ffbonded

bondtypes

i	j	func	b0 (nm)	kb (kJ/mol/nm^2)
CA	CV	1	0.146	322168
CA	CQ	1	0.151	265265.6
OBO	HOB	1	0.0972	3.70e+05;
B	OBO	1	0.138	4.19E+05
CBO	B	1	0.157	1.20E+05
CBO	CA	1	0.14	3.35E+05

angletypes

i	j	k	func	th0 (deg)	cth (kJ/mol/rad^2)
C_3	CT	C!	1	116	585.76
CT	CT	CA	1	116	585.76
CT	CT	C!	1	116	585.76
CT	CA	CA	1	120	711.28
CQ	CA	CA	1	120	711.28
CT	CA	HA	1	120	292.88
HA	CA	CT	1	120	292.88
CT	CA	C!	1	120	585.76
CA	C!	CT	1	120	585.76
CA	CQ	NC	1	124	585.76
CA	C_2	NC	1	124	585.76
CA	CV	CT	1	125	585.76
CQ	NC	NC	1	117	585.76
C_2	CA	CV	1	135	711.28
CR	NC	NC	1	135	711.28
CT	CA	CT	1	120	585.76
CT	C!	CT	1	120	585.76

NB	CR	NC	1	120	585.76
NC	CR	CT	1	125	585.76
CR	CT	HC	1	110	292.88
CT	CT	C!	1	114	527.18
C!	CT	HC	1	110	292.88
C_2	CA	NC	1	109	585.76
CV	CA	NC	1	109	585.76
B	OBO	HOB	1	110	399.86
CBO	B	OBO	1	124	501.73
CA	CBO	B	1	120	420.00
OBO	B	OBO	1	117	503.12
HA	CA	CBO	1	120	378.75
CBO	CA	CA	1	120	420.00
CBO	CA	C!	1	120	420.00
CA	CBO	CA	1	120	420.00

dihedraltypes

i	**j**	**k**	**l**	**func**	**coefficients** (kJ/mol)					
CA	CA	CQ	NC	3	0.8368	0	-0.8368	0	0	0
CQ	NC	C_2	O_2	3	0	0	0	0	0	0
CQ	NC	C_2	CA	3	0	0	0	0	0	0
C!	CA	CT	CT	3	0	0	0	0	0	0
CA	C!	CT	CT	3	0	0	0	0	0	0
CA	C!	CA	HA	3	0	0	0	0	0	0
CA	C!	CA	CA	3	0	0	0	0	0	0
CT	C!	CA	HA	3	0	0	0	0	0	0
CT	C!	CA	CA	3	0	0	0	0	0	0
HA	CA	CT	CT	3	0	0	0	0	0	0
C!	CA	CT	HC	3	0	0	0	0	0	0
HA	CA	CT	HC	3	0	0	0	0	0	0
CR	CT	CT	CT	3	2.9288	-1.4644	0.2092	-1.6736	0	0
C!	CT	CT	CT	3	2.9288	-1.4644	0.2092	-1.6736	0	0
CT	CA	CT	CT	3	0	0	0	0	0	0
CT	CA	CT	HC	3	0	0	0	0	0	0
N	CT	CT	NT	3	19.59994	-21.3907	4.05011	-2.25936	0	0
HA	NC	C_2	O_2	3	0	0	0	0	0	0
HA	NC	C_2	CA	3	0	0	0	0	0	0
NC	C_2	CA	CV	3	0	0	0	0	0	0
NC	C_2	CA	NC	3	0	0	0	0	0	0
O_2	C_2	CA	CV	3	0	0	0	0	0	0
O_2	C_2	CA	NC	3	0	0	0	0	0	0
C_2	CA	CV	NB	3	0	0	0	0	0	0
C_2	CA	CV	CT	3	0	0	0	0	0	0
NC	CA	CV	NB	3	0	0	0	0	0	0
NC	CA	CV	CT	3	0	0	0	0	0	0
HOB	OBO	B	OBO	3	0	0	0	0	0	0
HOB	OBO	B	CBO	3	0	0	0	0	0	0
OBO	B	CBO	CA	3	0	0	0	0	0	0
B	CBO	CA	HA	3	0	0	0	0	0	0
B	CBO	CA	C!	3	0	0	0	0	0	0
CA	CA	CBO	CA	3	0	0	0	0	0	0
CA	CBO	CA	C!	3	0	0	0	0	0	0
HA	CA	CBO	CA	3	0	0	0	0	0	0
CBO	CA	C!	CT	3	0	0	0	0	0	0
CBO	CA	C!	CA	3	0	0	0	0	0	0

B	CBO	CA	CA	3	0	0	0	0	0	0

2 Supplemental simulation results

In this section, we discuss our simulations results in more details. We first show the atomic structure of the initial configuration of the MA-ST polymer, as generated by Materials Studio, in Fig. S3a. In Fig. S3b and c, we show the reference polymer structure used for calculating the diffusion coefficient. This structure is obtained by simulating only the polymer in pure water, i.e., without the SWNT.

In Fig. S4, we show equilibrated atomic configurations of the MA-ST corona phase around the SWNT in the presence of water after an NPT simulation run. There is no Vardenafil in these simulations. The three structures shown correspond to three different simulation runs. Since we used random velocity generation at the start of the NVT runs in these simulations, the starting configuration of the system is different in each case. In Fig. S5, we have extended the NPT simulation of the polymer corona by 50 ns, and the result shows a similar polymer configuration. In Fig. S6, we show the properties of the polymer corona in the three simulation runs. We see that the polymer end-to-end distance, polymer-SWNT LJ interaction, SWNT solvent accessible surface area, and the temperature are consistent among the three runs. Since the initial configurations are different, the consistent results from different runs indicate that the simulation has reached thermal and density equilibrium.

In Fig. S7, we show equilibrated atomic configurations of the MA-ST corona phase in the presence of Vardenafil along with water after an NPT simulation run. The three structures shown correspond to three different simulation runs. Since we used random velocity generation at the start of the NVT runs in these simulations, the starting configuration of the system is different in each case. In Fig. S8, we show the properties of the polymer corona in the three simulation runs. We see that the polymer end-to-end distance, polymer-Vardenafil LJ interaction, SWNT solvent accessible surface area, and the temperature are consistent among the three runs. Since the initial configurations are different, the consistent results from different runs indicate that the simulation has reached thermal and density equilibrium.

In Fig. S9, we depict structures of three different configurations at different times of the last 10 ns of the simulation run. The three configurations spread over 10 ns of simulation time only have minor structural differences between them.

In Fig. S10, S11, and S12, we explore the simulation time of the NVT and the NPT runs, on the results obtained. In all three simulation scenarios, the system has reached thermal and density equilibrium in the last 10 ns.

In Fig. S13 and S14, we show the results of two new simulations with different initial configurations. The resulting configurations are similar to the results in Fig. S4, which starts with an initial configuration shown in Fig. S3.

In Fig. S15, we show the mean square displacement plots of free MA-ST polymer and Vardenafil, and the calculation of their diffusion coefficients. There, we also compare the simulated diffusion coefficients with values calculated using the Stokes-Einstein equation, showing good agreement between the two sets of values, thereby indicating the force fields we have used to be appropriate.

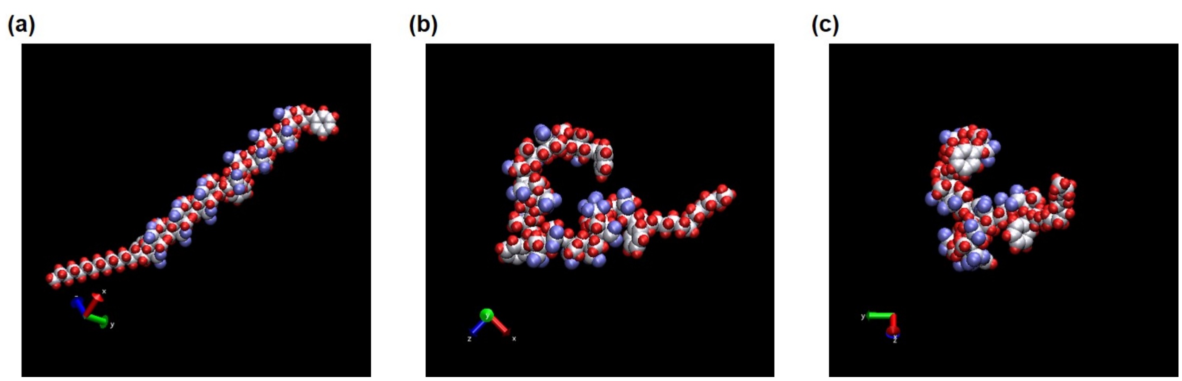

Figure S3: (a), The initial configuration of MA-ST polymer, generated by Materials Studio. The distance between polymer and nanotube centers of mass is 2.21 nm. (b) and (c), The screensnaps of a reference polymer configuration from two angles. The configuration is generated by simulating the free MA-ST polymer in water for 1 ns NVT and 20 ns NPT, in the absence of nanotubes. The free polymer simulation is used estimate the diffusion coefficient of the polymer. Water molecules have been omitted from the snapshots for clarity. Atom colors: C - silver, O - blue, H - red.

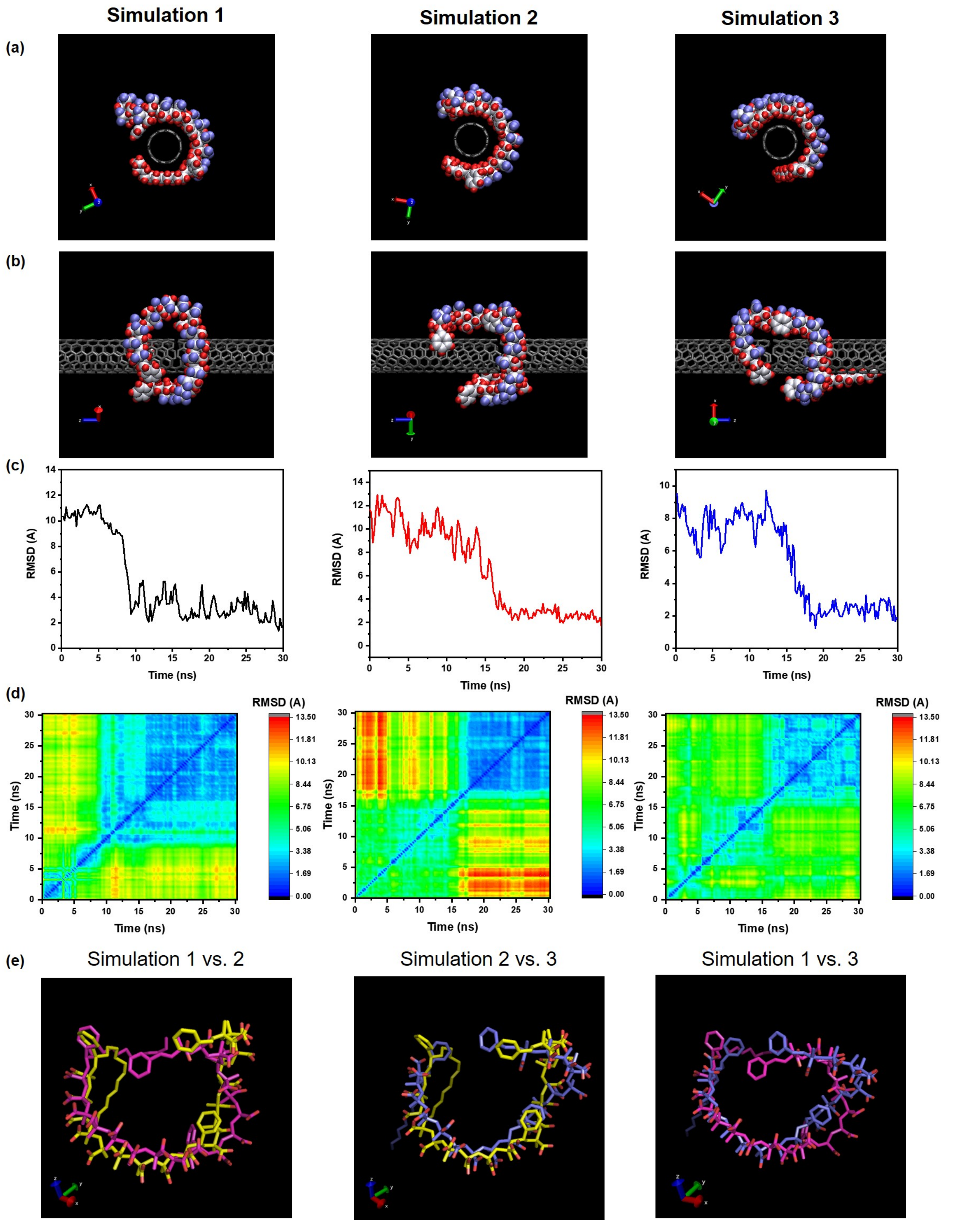

Figure S4: Equilibrium configurations of independent simulations for MA-ST-90 corona phase, including the cross section (a) and the side view (b). The RMSD evolution during the NPT simulation is plotted in (c), where the polymer trajectory is referenced to the shown

Figure S4: (Continued) configuration in (a) and (b). The RMSD equilibrates after about 15-20 ns and fluctuates only by ± 1 Å. Therefore, we can now conclude that the polymer configurations have reached equilibrium. (d) 2D RMSD plots shows the evolution of RMSD for any two configurations selected from the simulation trajectory. Again, the plots show that in the last 10 ns of the respective simulations, the RMSD values are stable and close to 2 Å, hence the configurations in the last 10 ns are stable. (e) To compare the resulting polymer configurations among different runs, the overlays of the resulting configurations are shown. Since we used random velocity generation at the start of the NVT runs in these simulations, the starting configuration of the system is different in each case. The resulting polymer configuration among the runs are very similar. The polymer RMSD between simulations are: Simulation 1 vs. 2 is 0.43 nm; Simulation 2 vs. 3 is 0.46 nm; Simulation 1 vs. 3 is 0.51 nm. Water molecules have been omitted from the snapshots for clarity. Atom colors in (a) and (b): C in nanotubes - grey, C in polymer - silver, O - blue, H - red. Atom colors in (e): C in Simulation 1 - pink, C in Simulation 2 - yellow, C in Simulation 3 - purple, O - red, H - not shown.

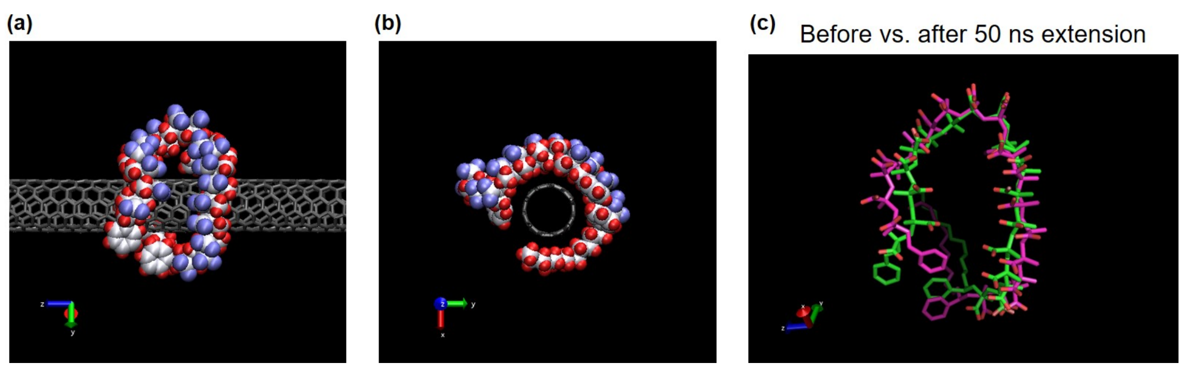

Figure S5: When the NPT simulation of the MA-ST-90 polymer corona is extended by 50 ns, the resulting configuration is similar to that of it without the 50 ns extension. (a) and (b), The side view and cross section of the configuration after extending the NPT simulation by 50 ns, based on Simulation 1 in Fig. S4. (c), The overlay of the polymer configurations before and after the 50 ns extension, where the configuration without the extension has carbon atoms in pink, and the configuration afterwards has carbon atoms in green. The RMSD between these configurations is 2.81 Å. From the comparison, one can infer that the structure of the polymer-SWNT binding pocket does not change even if a longer MD simulation is considered. Water molecules have been omitted from the snapshots for clarity. Atom colors in (a) and (b): C in nanotubes - grey, C in polymer - silver, O - blue, H - red. Atom colors in (c): C in before 50 ns extension - pink, C in after 50 ns extension - green, O - red, H - not shown.

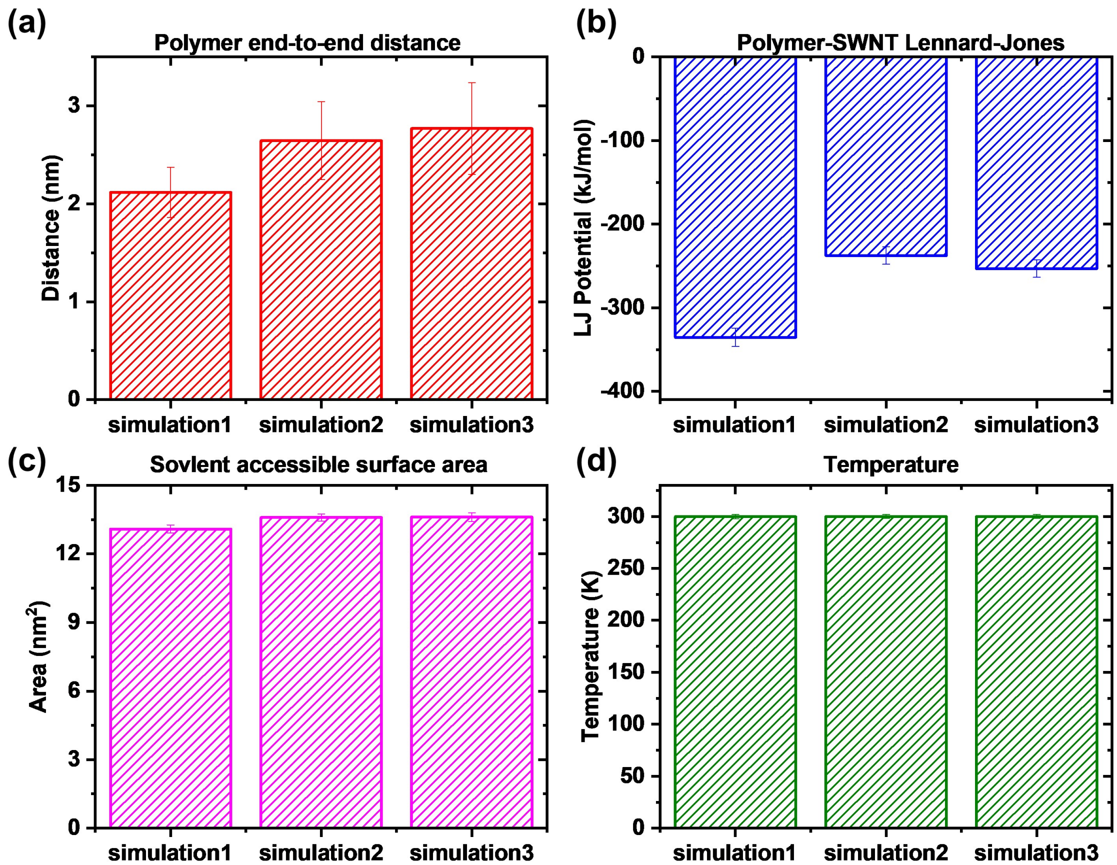

Figure S6: Property comparisons among independent simulations for MA-ST corona phase, in the absence of analyte. Each simulation is composed of 40 ns NVT followed by 30 ns NPT simulation, with different starting configuration. The polymer end-to-end distance (a), the polymer-nanotube Lennard-Jones potential (b), the SWNT solvent accessible surface area (c), and the temperature (d) are compared among the three simulations. The last 10 ns out of the 70 ns simulations are used for analysis, where the average and the standard deviation during this 10 ns are plotted. The values of these properties are similar among the simulations, suggesting the simulations have reached equilibrium.

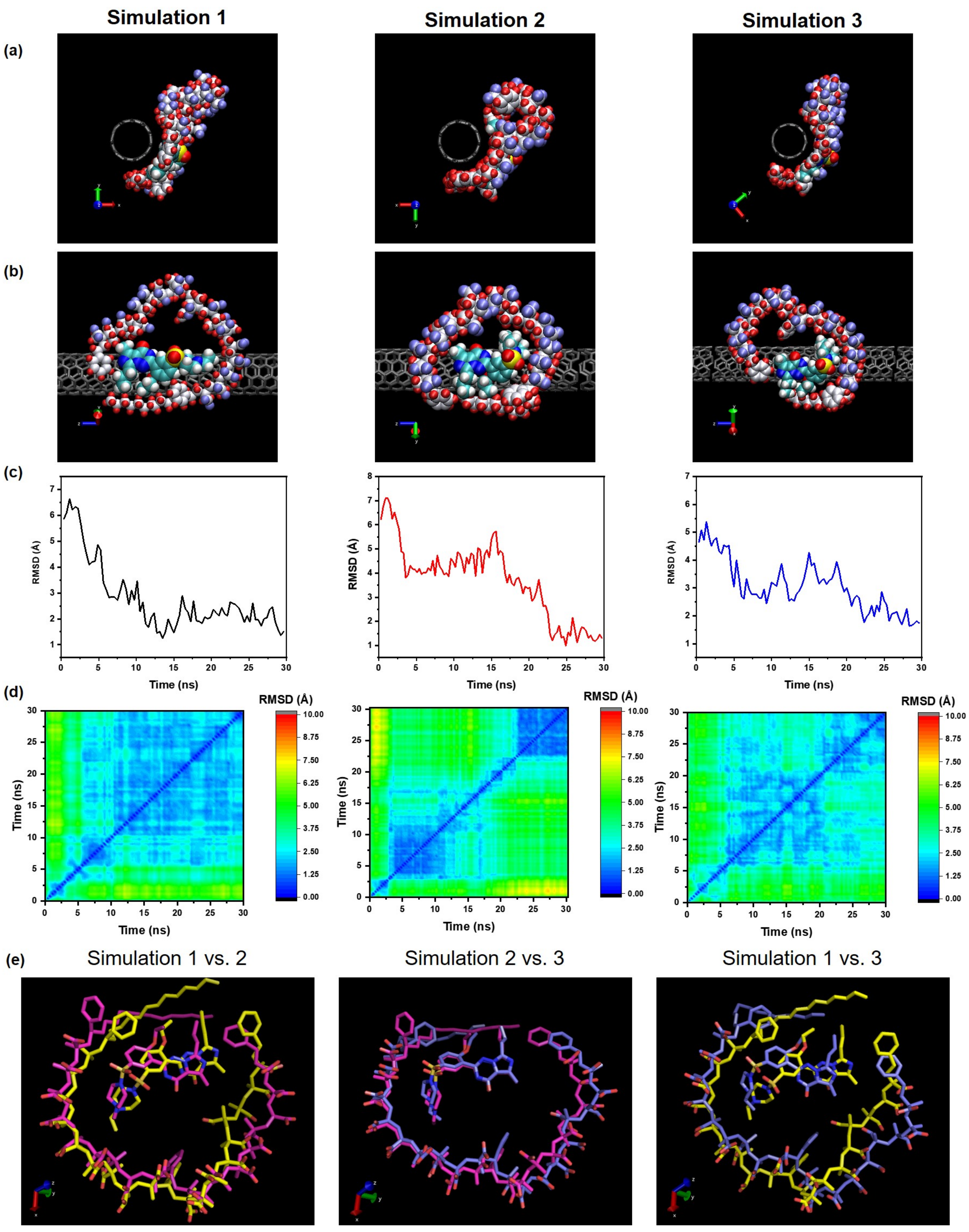

Figure S7: Equilibrium configurations of independent simulations for the interaction between the corona phase and the Vardenafil, including the cross section (a) and the side view (b). The RMSD evolution during the NPT simulation is plotted in (c), where the polymer trajectory is referenced to the shown configuration in (a) and (b). The RMSD equilibrates

Figure S7: (continued) after about 15-22 ns and fluctuates by ± 1 Å. Therefore, we can now conclude that the corona-drug configurations have reached equilibrium. (d) 2D RMSD plots shows the evolution of RMSD for any two configurations selected from the simulation trajectory. Again, the plots show that in the last 8 ns of the respective simulations, the RMSD values are stable and less than 2.5 Å, hence the configurations in the last 8 ns are stable. (e) To compare the resulting corona-drug configurations among different runs, the overlays of these configurations are shown. Since we used random velocity generation at the start of the NVT runs in these simulations, the starting configuration of the system is different in each case. The shapes of the corona phase, the docking configuration of Vardenafil, and the relative position of Vardenafil to the corona phase are consistent among the three simulations. The RMSD between simulations are: Simulation 1 vs. 2 is 0.24 nm; Simulation 2 vs. 3 is 0.23 nm; Simulation 1 vs. 3 is 0.34 nm. Water molecules have been omitted from the snapshots for clarity. Atom color in nanotubes in (a) and (b): C - grey. Atom colors in polymer in (a) and (b): C - silver, O - blue, H - red. Atom colors in Vardenafil in (a) and (b): C - green, O - red, S - yellow, N - dark blue, H - white. Atom colors in (e): C in Simulation 1 - pink, C in Simulation 2 - yellow, C in Simulation 3 - purple, O - red, S – orange, N – blue, H - not shown.

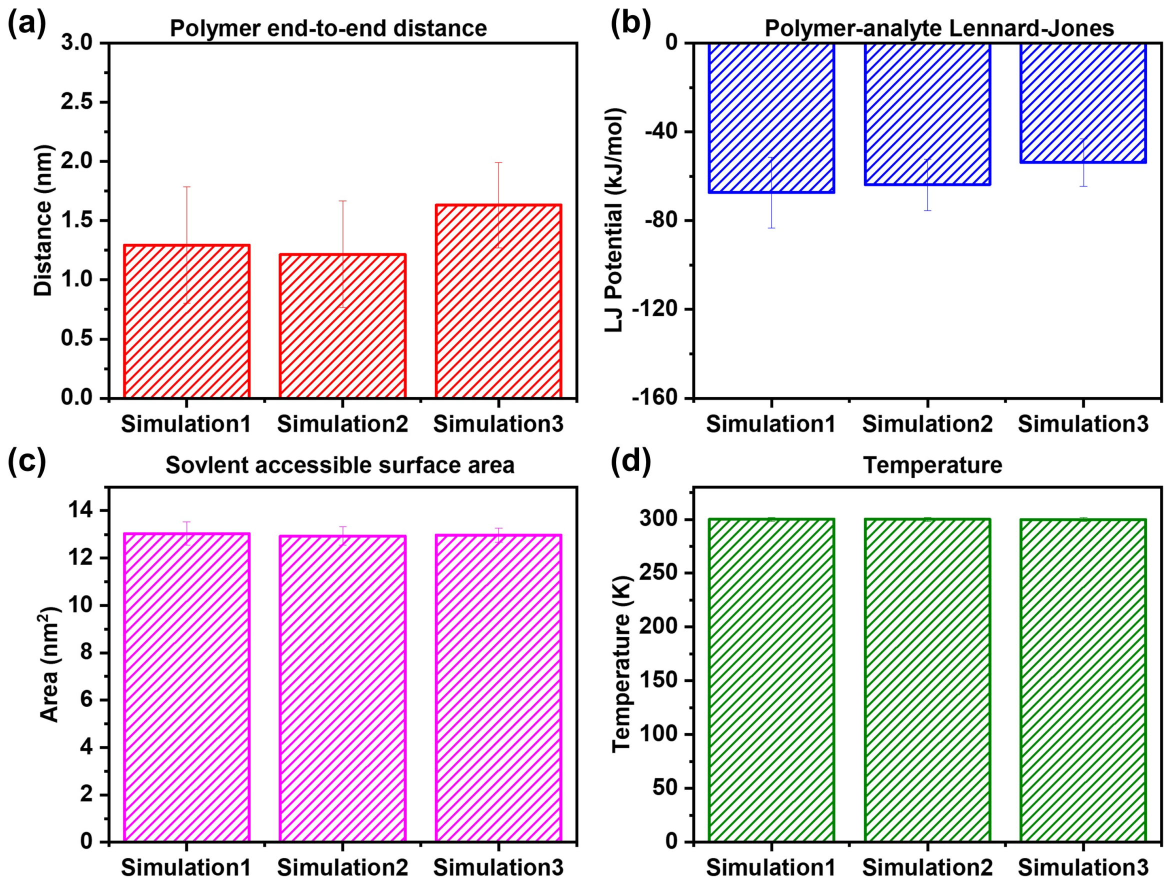

Figure S8: Property comparisons among independent simulations for the interaction between the corona phase and the analyte Vardenafil. The polymer end-to-end distance (a), the polymer-Vardenafil Lennard-Jones potential (b), the SWNT solvent accessible surface area (c), and the temperature (d) are compared among the three simulations. The last 10 ns out of the 70 ns simulations are used for analysis, where the average and the standard deviation during this 10 ns are plotted. The values of these properties are similar among the simulations, suggesting the simulations have reached equilibrium.

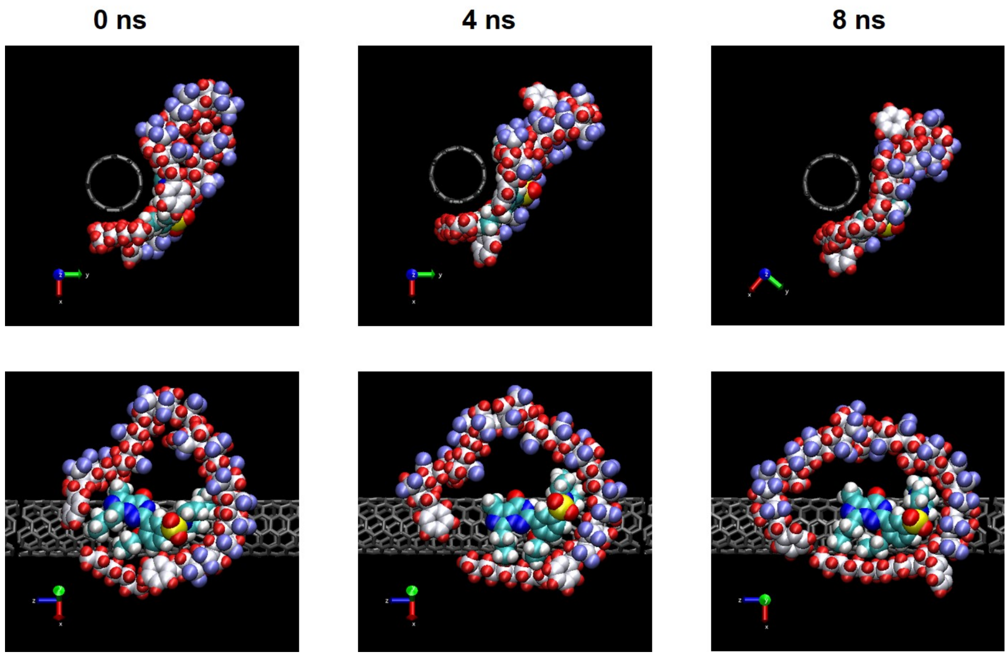

Figure S9: The configurations of the MA-ST corona phase interacting with the analyte at different time points (0, 4, and 8 ns) during the last 10 ns of simulation. Throughout this stage, Vardenafil always docks in the binding pocket, and the intermolecular interactions between the corona phase and the analyte are consistent. Thus, the configurations are good representations of the final configuration. Water molecules have been omitted from the snapshots for clarity. Atom color in nanotubes: C - grey. Atom colors in polymer: C - silver, O - blue, H - red. Atom colors in Vardenafil: C - green, O - red, S - yellow, N - dark blue, H - white.

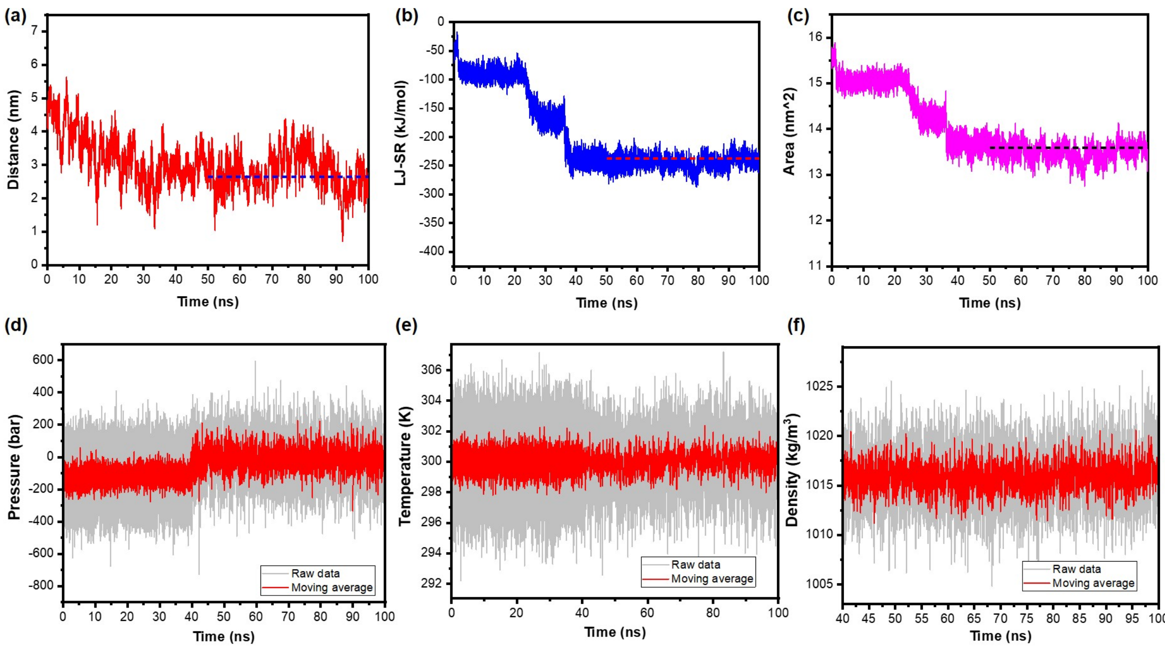

Figure S10: Simulation time investigation. A 100 ns simulation (40 ns NVT + 60 ns NPT) of the corona phase was carried out to examine the configuration of polymer around SWNTs, in the presence of water. The evolution of its properties over the simulation time is shown, including the polymer end-to-end distance (a), the polymer-nanotube Lennard-Jones potential (b), the solvent accessible area of nanotubes (c), the pressure (d), the temperature (e), and the density of the system during the NPT part (f). All are stable after 50 ns, indicating the system has reached equilibrium. The dash lines are the average value for frames between 90 ns and 100 ns.

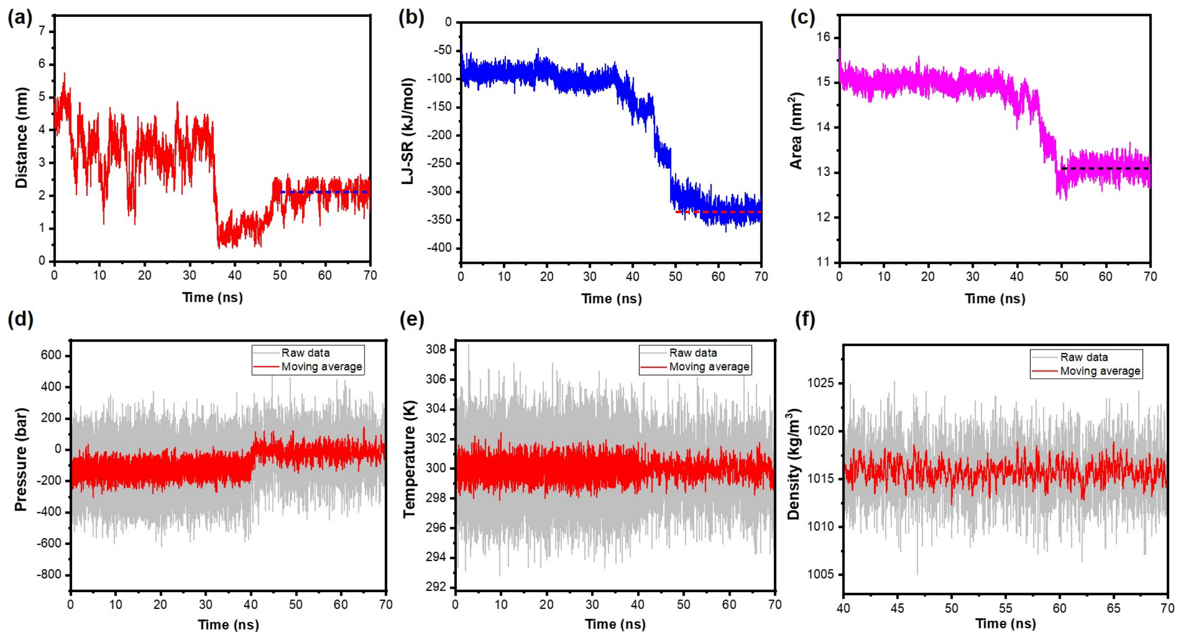

Figure S11: An example of the corona phase simulation, which examines the configuration of polymer around SWNTs, demonstrates that the system has reached equilibrium within 70 ns. The 70 ns simulation composes of 40 ns NVT and 30 ns NPT. The polymer end-to-end distance (a), the polymer-nanotube Lennard-Jones potential (b), the solvent accessible area of nanotubes (c), the pressure (d), the temperature (e), and the density of the system during the NPT part (f) are stable after 50 ns, indicating the system has reached equilibrium. The dash lines are the average value for frames between 60 ns and 70 ns.

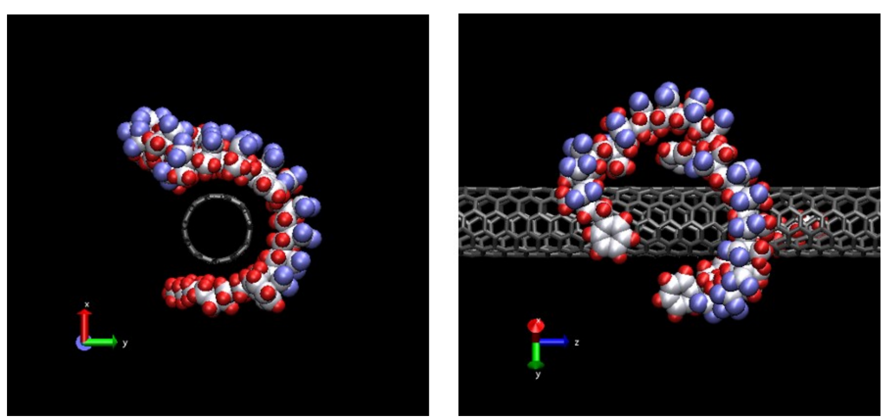

Figure S12: The screensnaps of a simulation using short NVT show similar results as the one with long NVT. The simulation is carried out with 1 ns NVT and 60 ns NPT, and the resulting configuration is consistent with the one using 40 ns NVT, as in Fig. S10. Properties of the state: polymer-nanotube Lennard-Jones potential is -317 kJ/mol; polymer end-to-end distance is 2.37 nm; and solvent accessible surface area is 13.01 nm^2. Left image: head view. Right image: side view. Water molecules have been omitted from the snapshots for clarity. Atom color in nanotubes: C - grey. Atom colors in polymer: C - silver, O - blue, H - red.

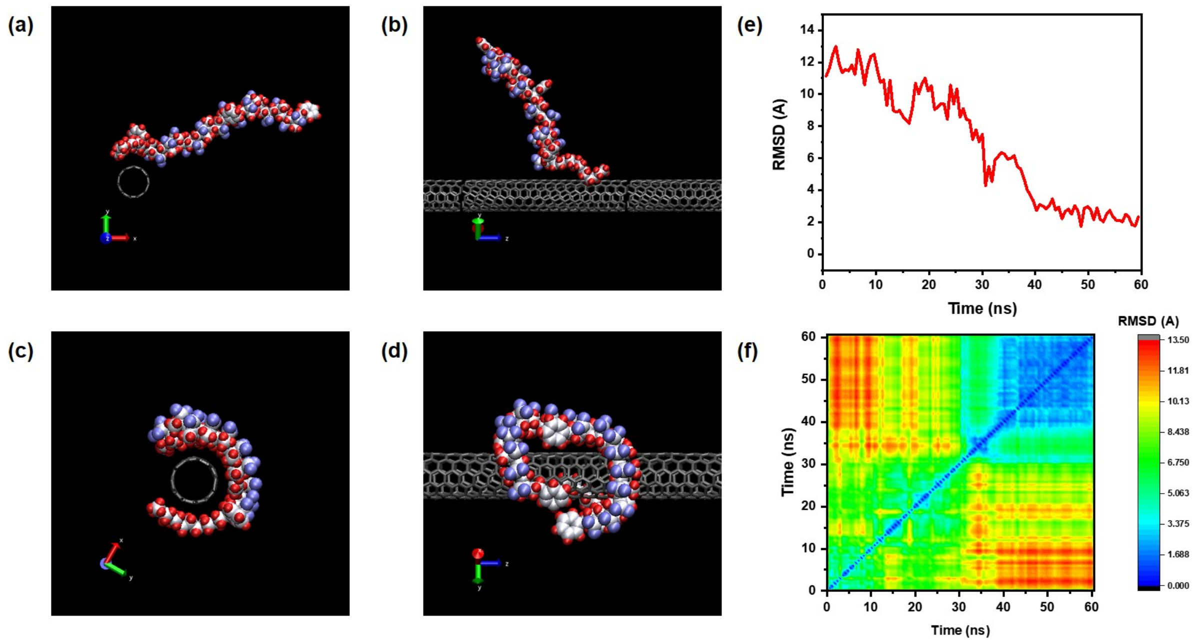

Figure S13: MA-ST corona phase configuration simulation with a different starting configuration. The cross section (a) and the side view (b) of the starting configuration. The distance between polymer and nanotube centers of mass is 2.42 nm at the start of the simulation. The cross section (c) and the side view (d) of the resulting configuration, after 1 ns of NVT and 60 ns of NPT simulation. Properties of the state: polymer-nanotube Lennard-Jones potential is -370 kJ/mol; polymer end-to-end distance is 1.78 nm; and solvent accessible surface area is 12.98 nm^2. The RMSD evolution during the NPT simulation is plotted in (e), where the polymer trajectory is referenced to the shown configuration in (c) and (d). (f) 2D RMSD plots shows the evolution of RMSD for any two configurations selected from the simulation trajectory. The plots show that in the last 20 ns of the simulations, the RMSD values are stable and close to 2 Å, hence the configurations in the last 20 ns are stable. The RMSD of the resulting configuration compared to Simulation 1 in Fig. S4 is 3.00 Å, indicating that with the two different staring polymer configurations, the simulations have reached similar resulting polymer configurations. Water molecules have been omitted from the snapshots for clarity. Atom color in nanotubes: C - grey. Atom colors in polymer: C - silver, O - blue, H - red.

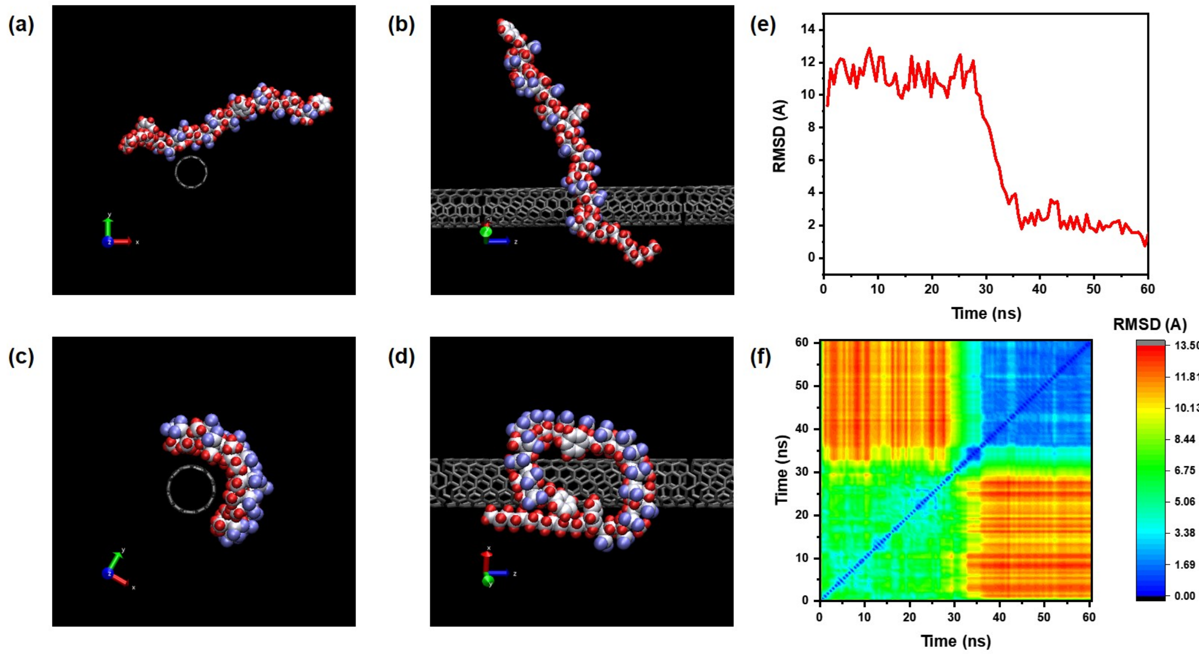

Figure S14: MA-ST corona phase configuration simulation with a third starting configuration. The cross section (a) and the side view (b) of the starting configuration. The distance between polymer and nanotube centers of mass is 1.44 nm at the start of the simulation. The cross section (c) and the side view (d) of the resulting configuration, after 1 ns of NVT and 60 ns of NPT simulation. Properties of the state: polymer-nanotube Lennard-Jones potential is -347 kJ/mol; polymer end-to-end distance is 1.23 nm; and solvent accessible surface area is 11.79 nm^2. The RMSD evolution during the NPT simulation is plotted in (e), where the polymer trajectory is referenced to the shown configuration in (c) and (d). (f) 2D RMSD plots shows the evolution of RMSD for any two configurations selected from the simulation trajectory. The plots show that in the last 20 ns of the simulations, the RMSD values are stable and close to 1.7 Å, hence the configurations in the last 20 ns are stable. The RMSD of the resulting configuration compared to Simulation 1 in Fig. S4 is 3.97 Å, indicating that with the two different staring polymer configurations, the simulations have reached similar resulting polymer configurations. Water molecules have been omitted from the snapshots for clarity. Atom color in nanotubes: C - grey. Atom colors in polymer: C - silver, O - blue, H - red.

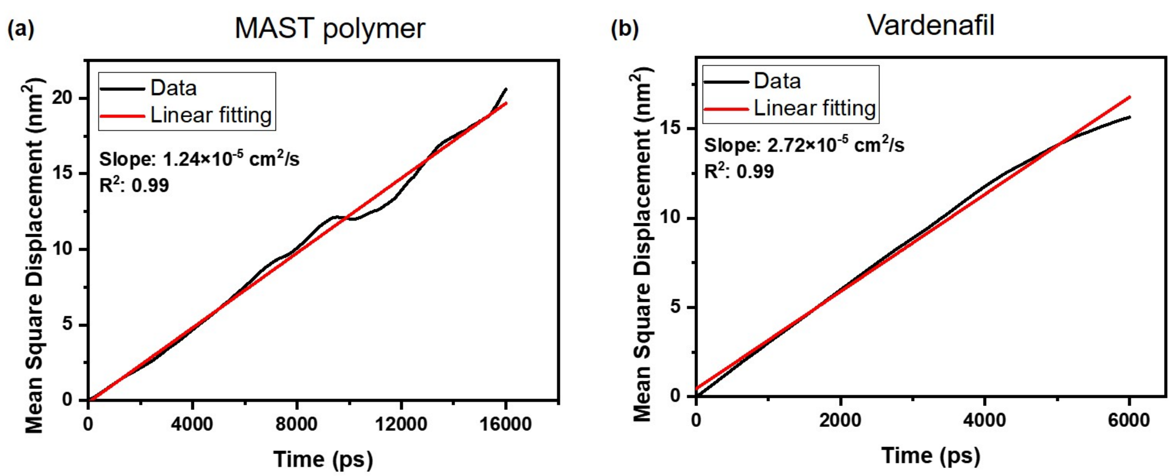

Figure S15: Mean square displacement (MSD) plots for MAST polymer (a) and Vardenafil (b). The MSDs are calculated based on the center of mass positions, using GROMACS, in a control system where the polymer or the drug diffuse freely in water without the presence of nanotubes. These plots are used to estimate the diffusion coefficient based on the Einstein relation, where in the plot of MSD vs. t, the slope is 6 times of diffusion coefficient D. The estimated D for MAST polymer is $0.207 \times 10^{-5}\, cm^2/s$. For Vardenafil, it is $0.453 \times 10^{-5}\, cm^2/s$.

The theoretical values of diffusion coefficients are calculated using Stokes-Einstein equation, $D = k \times T/(6 \times \pi \times r \times \eta)$, where k is the Boltzmann constant, T is the temperature (300 K), r is the radius of the molecule, and η is the liquid viscosity ($0.001\, N \times s/m^2$ for water). The radii of the molecules are estimated based on their configurations in free water (1.01 nm for polymer and 0.47 nm for Vardenafil). The resulting theoretical D of polymer and Vardenafil are $0.216 \times 10^{-5}\, cm^2/s$ and $0.466 \times 10^{-5}\, cm^2/s$, respectively. The calculated diffusion coefficients based on the simulations are very close to their respective theoretical values, indicating the two force fields we have used - OPLS-AA for polymer and GROMOS54A7 for Vardenafil - seem reasonable.

3 Nanotube surface coverage characterization

Solvatochromic shift

To estimate the nanotube surface coverage by polymer corona, we used a semiempirical model developed previously.[S17,S18] As shown in Fig.4b in the main text, the product of transition energy (E_{11}^2) and transition energy shift (ΔE_{11}) is inversely related to nanotubes' diameter (d^{-4}, where d is the diameter), where the slope of the linear fitting, c, is a function of the effective dielectric constant according to Eqn (1). By comparing the slope with that of a reference system of known dielectric constant (ε_{ref}) and reflective index(η_{ref}), we can calculate the effective dielectric constant of our corona phases(ε_{eff}, Eqn (2)). By assuming a linear combination of water and polymer contribution, the surface coverage of SWNTs (α) is thus calculated (Eqn (3)).

The reference system is wrapped by N-methyl-2-pyrrolidone, where $c_{ref} = 0.060\, eV^3 nm^4$, $\varepsilon_{ref} = 32.2$ and $\eta_{ref} = 1.47$.[S18] Assume that polymers have similar refractive index as water($\eta = 1.333$) and the dielectric constant is 3.0.[S19]

$$(E_{11})^2 \Delta E_{11} = -Lk[\frac{2(\varepsilon - 1)}{2\varepsilon + 1} - \frac{2(\eta^2 - 1)}{2\eta^2 + 1}](\frac{1}{d^4}) = \frac{c}{d^4} \tag{1}$$

$$\frac{c}{c_{ref}} = \frac{\frac{\varepsilon_{eff} - 1}{2\varepsilon_{eff} + 1} - \frac{\eta^2 - 1}{2\eta^2 + 1}}{\frac{\varepsilon_{ref} - 1}{2\varepsilon_{ref} + 1} - \frac{\eta_{ref}^2 - 1}{2\eta_{ref}^2 + 1}} \tag{2}$$

$$\varepsilon_{eff} = \alpha\varepsilon_{polymer} + (1 - \alpha)\varepsilon_{water} \tag{3}$$

Dye adsorption quantification

Riboflavin adsorption model

Riboflavin adsorption model is derived following the Langmuir adsorption model. Assume the free riboflavin concentration is c_{free}, the concentration of adsorbed riboflavin is c_{ads}, the total concentration of riboflavin is c_{total}, the total number of vacant sites on polymer wrapped SWNT is q (per carbon atom), the total concentration of vacant sites on SWNT is θ_t, the concentration of riboflavin adsorbed sites on SWNT is θ_a, the concentration of exposed sites after riboflavin adsorption is θ_e, the forward reaction rate is k_{on}, the backward reaction rate is k_{off}, the dissociation constant of dye binding to SWNT is $K_{SWNT-dye}$, and the SWNT concentration on a carbon atom basis is C_{SWNT}.

$$c_{free} + \theta_e \underset{\text{kon}}{\overset{\text{koff}}{\Longleftrightarrow}} \theta_a$$

$\because$ At equilibrium, the forward and backward reactions have the same rate,

$\therefore k_{on} \cdot c_{free} \cdot \theta_e = k_{off} \cdot \theta_a$

$\because \theta_a + \theta_e = \theta_t$, and $K_{SWNT-dye} = k_{off}/k_{on}$, the above equation can be converted to:

$$c_{free}(\theta_t - \theta_a) = K_{SWNT-dye} \cdot \theta_a$$

$$c_{free} \cdot \theta_t = (K_{SWNT-dye} + c_{free})\theta_a$$

$$\frac{\theta_a}{\theta_t} = \frac{c_{free}}{K_{SWNT-dye} + c_{free}}$$

The above equation shows the fraction of vacant sites that are adsorbed with riboflavin. Because the concentration of vacant sites (θ_t) equals $C_{SWNT} \cdot q$, the amount of riboflavin adsorbed is:

$$c_{ads} = C_{SWNT} \cdot q \cdot \frac{c_{free}}{K_{SWNT-dye} + c_{free}}$$

$$\frac{C_{SWNT}}{c_{ads}} = \frac{K_{SWNT-dye} + c_{free}}{c_{free} \cdot q} = \frac{K_{SWNT-dye}}{q} \cdot \frac{1}{c_{free}} + \frac{1}{q} \tag{4}$$

The total riboflavin concentration in the solution is:

$$c_{total} = c_{free} + c_{ads} = c_{free} + C_{SWNT} \cdot q \cdot \frac{c_{free}}{K_{SWNT-dye} + c_{free}}$$

Riboflavin fluorescence-adsorption correlation

The riboflavin fluorescence intensity is linearly proportional to the concentration of free riboflavin in solution. If we assume the linear constant is a, in the control group, without riboflavin adsorption, the fluorescence intensity (I_{ctrl}) is:

$$I_{ctrl} = a \cdot c_{free} = a \cdot c_{total};$$
$$a = \frac{I_{ctrl}}{c_{total}}$$

In the SWNT solution, the corresponding riboflavin fluorescence intensity in the solution (I_{swnt}) is:

$$I_{swnt} = a \cdot c_{free}$$

Since the difference in intensity is related to the adsorbed riboflavin (Δ), c_{ads} can be calculated by:

$$\Delta = I_{ctrl} - I_{swnt} = a(c_{total} - c_{free}) = a \cdot c_{ads}$$
$$c_{abs} = \frac{\Delta}{a} = \frac{\Delta}{I_{ctrl}} \cdot c_{total}$$

The resulting c_{ads} can be used in Equation (4) to plot the linear correlation between $\frac{C_{SWNT}}{c_{ads}}$ and $\frac{1}{c_{free}}$, as in Figure 4 in the main text.

4 Supplementary results

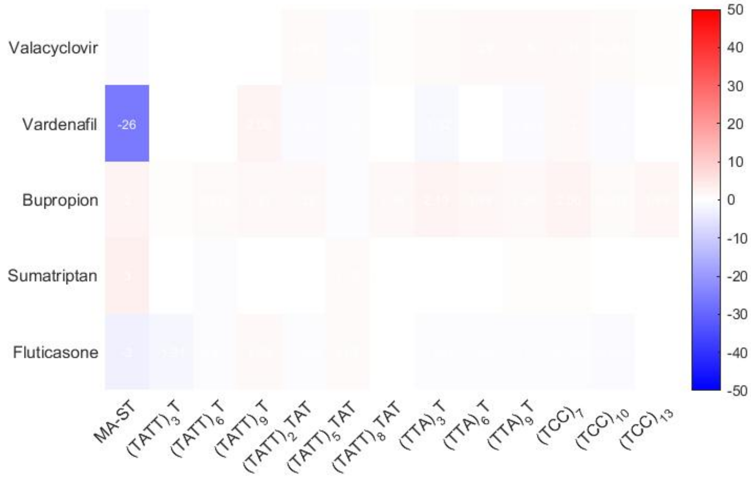

Figure S16: A library of single stranded DNAs was screened for potential recognition corona phase for target therapeutics. No recognition interaction was revealed.

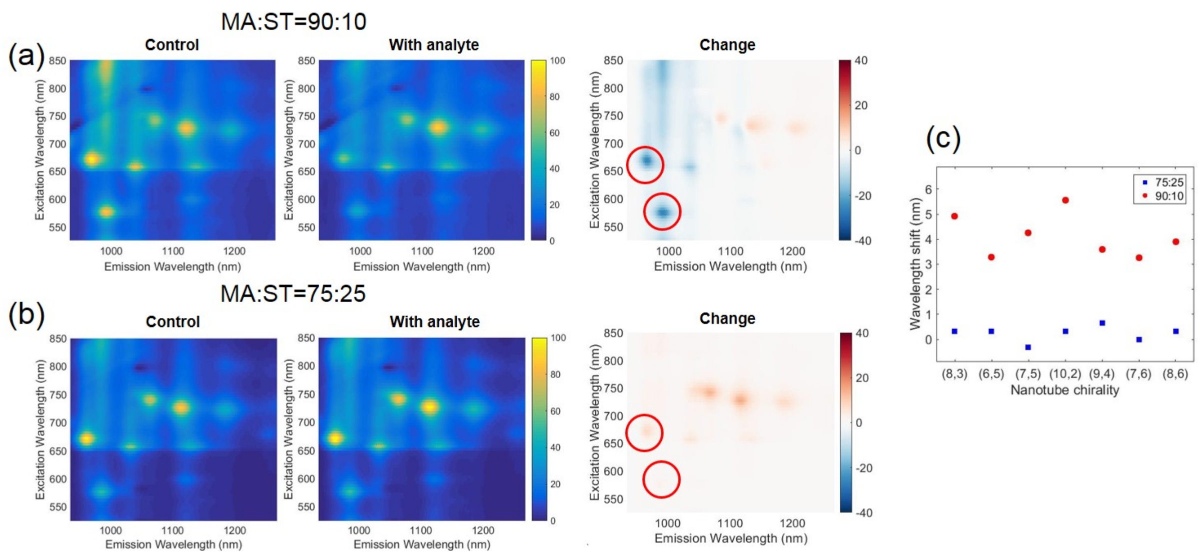

Figure S17: In forming a recognition configuration for Vardenafil, it is essential to have a large hydrophilic component in polymer composition. (a), Excitation-emission spectra of SWNTs with MA-ST-90 corona phase, including the spectrum before and after adding analyte, and the change of spectrum. The red circles highlight the (8,3) and (6,5) chirality that have the strongest response. (b), Excitation-emission spectra of MA-ST-75, where the spectral change is much less substantial, indicating the preference of a high hydrophilic component. The high hydrophilic component provides structural flexibility that promotes the recognition. (c), In comparison to MA-ST-75, the MA-ST-90 corona SWNTs experience larger emission wavelength shifts, indicating stronger interactions with analyte, a similar conclusion as of the emission intensity change.

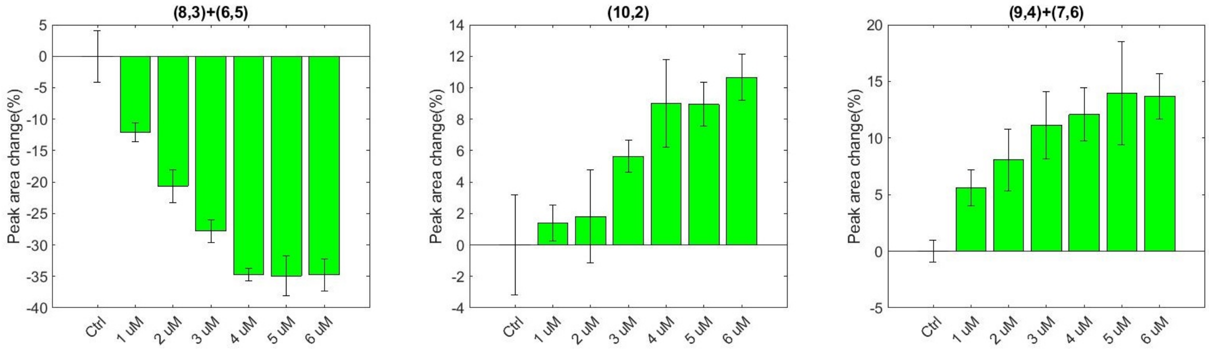

Figure S18: For MA-ST-90 corona, by comparing the emission intensity in NIR spectra, the corona phases of (6,5) and (8,3) chirality have the strongest recognition response, much higher than the corona phases of (10,2), (9,4) and (7,6) chirality. The recognition interaction has a preference for small diameter nanotubes.

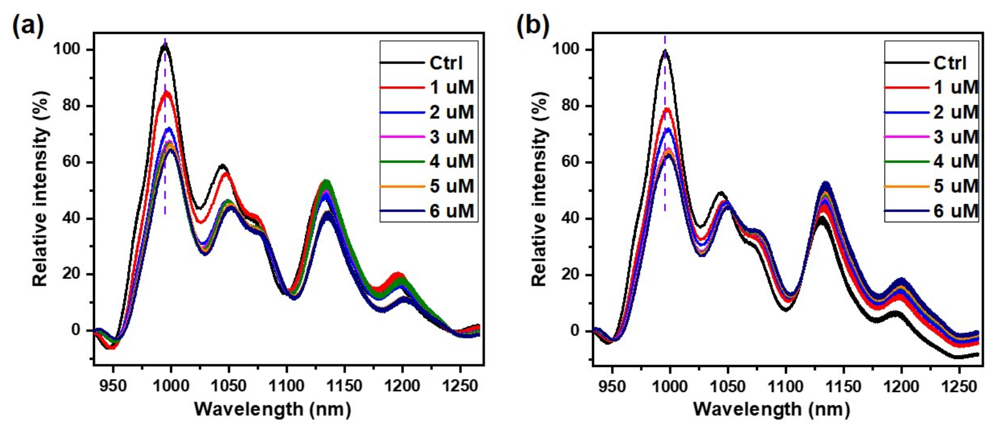

Figure S19: Batch-to-batch reproducibility of sensing responses. (a), The fluorescence emission spectra of nanotubes with MA-ST-90 corona, show a gradual intensity reduction when Vardenafil of 1 - 6 μM is introduced. Same plot as Fig. 3c. (b), Under the same condition, another batch of nanotubes with MA-ST-90 corona phase shows similar spectral change as the ones in part (a). The batch-to-batch variation of intensity change is 5-15%, and the trend is consistent, demonstrating a good reproducibility.

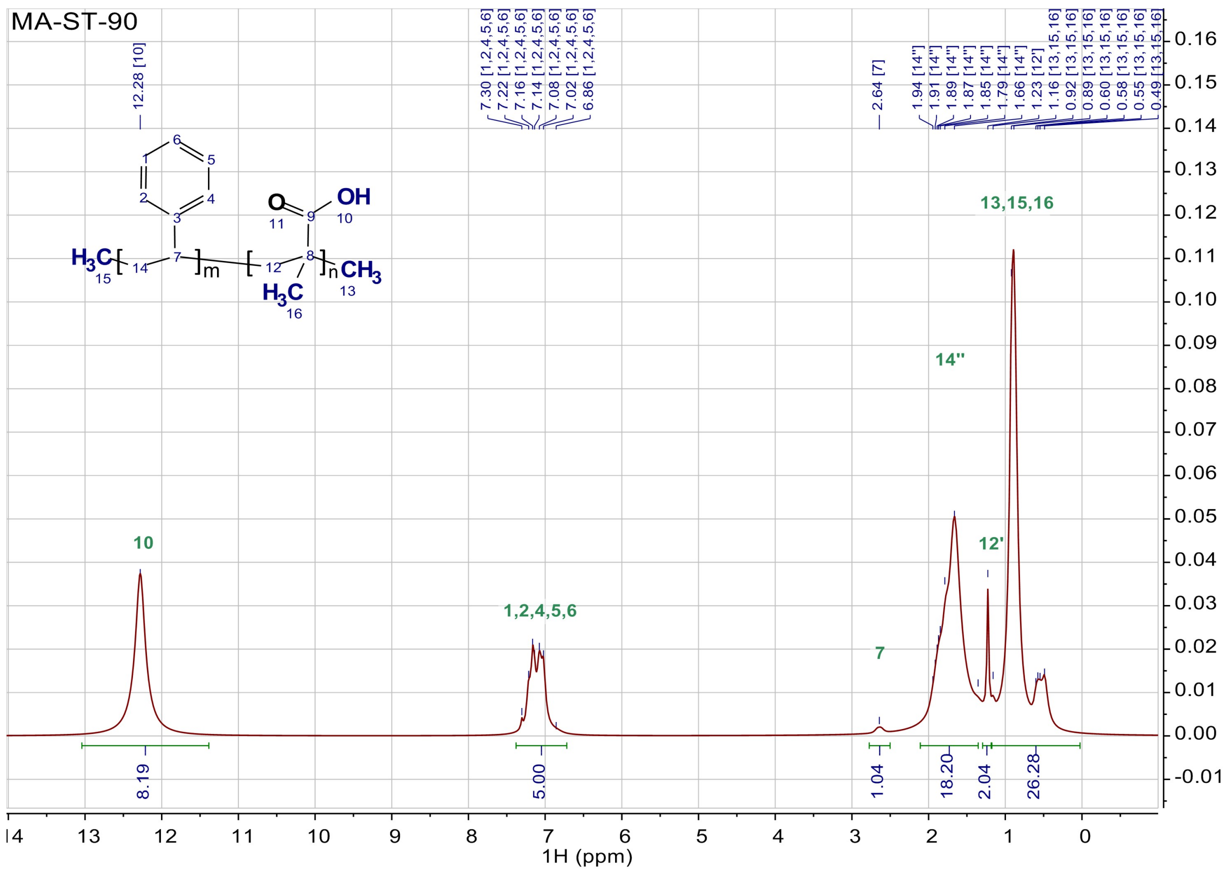

Figure S20: ^{1}H NMR spectrum of MA-ST-90 polymer. ^{1}H NMR (500 MHz, DMSO-d6): δ = 12.28 (s, 8H), 7.48 - 6.68 (m, 5H), 2.77 - 2.51 (m, 1H), 2.11 - 1.35 (m, 18H), 1.29 - 1.19 (m, 2H), 1.18 - 0.02 (m, 27H). ^{13}C NMR (126 MHz, DMSO-d6): δ = 179.29 (d, J = 88.0 Hz), 128.05 (s), 46.73 - 42.96 (m), 29.08, 17.13 (d, J = 201.8 Hz).

Table S2: Monomer peak integrals and conversion rates

		MA (2H)	**ST (1H)**	**Dioxane**	**Conversion(%)**		**MA:ST ratio**	
	δ:	5.95 & 5.47	6.60	3.53	MA	ST		
MA-ST-90	before	22.45	1.09	407.67				
	after	2	0	407.67	91.09	100.00	**9.38**	**1.00**
MA-ST-75	before	2.78	0.31	56.64				
	after	2	0.17	56.64	28.06	45.16	**2.79**	**1.00**

Monomer conversion rate is calculated by comparing the monomer abundance in the mixture before and after the reaction. The integrals of C=C bond peaks in monomers (δ = 5.95 and 5.47 for methacrylic acid and δ = 6.60 for styrene) were compared with the integral of the solvent peak (δ = 3.53 for dioxane). These ratios were used to calculate the conversion of each monomers, thus the monomer ratios (last column) in the polymers were calculated.

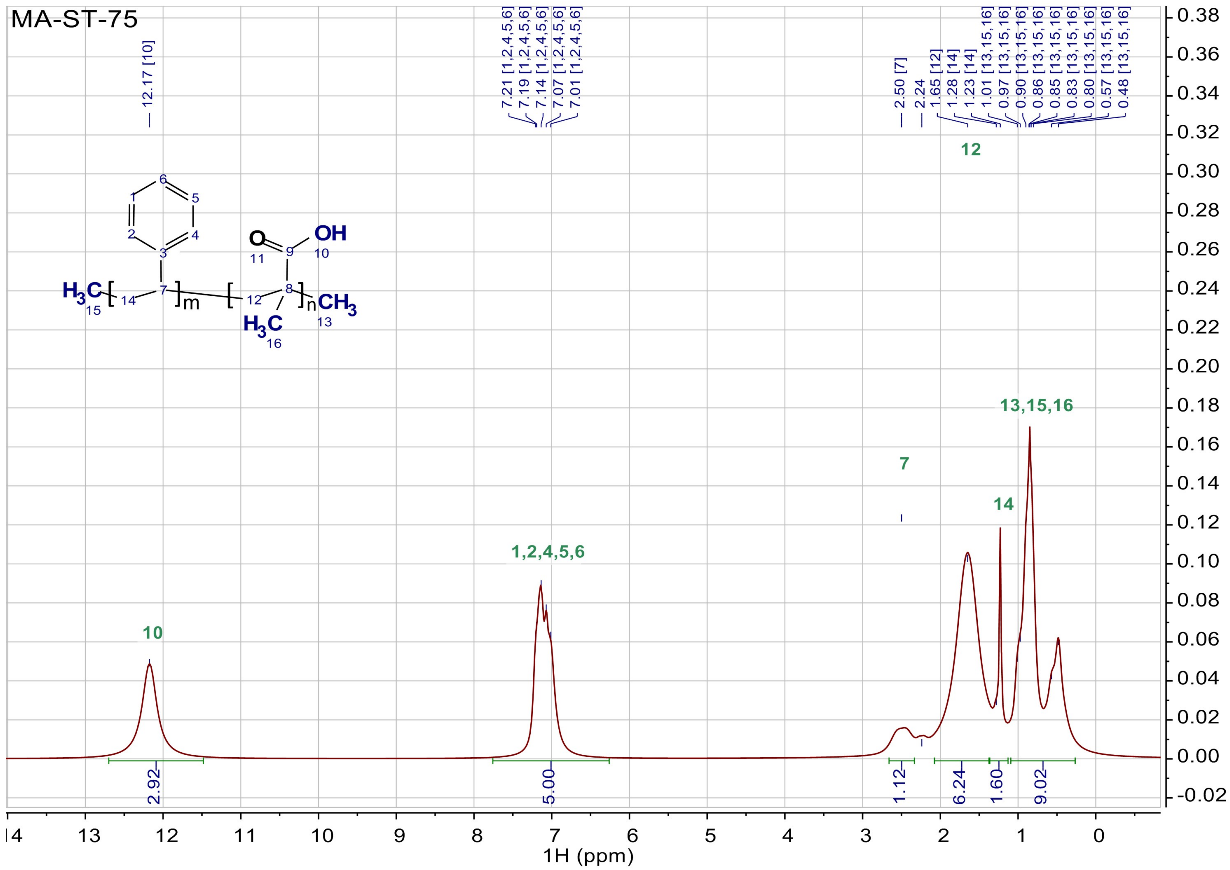

Figure S21: ^{1}H NMR spectrum of MA-ST-75 polymer. ^{1}H NMR (500 MHz, DMSO-d6): δ = 12.17 (s, 3H), 7.74 - 6.27 (m, 5H), 2.68 - 2.34 (m, 1H), 2.07 - 1.37 (m, 6H), 1.37 - 1.11 (m, 2H), 1.09 - 0.25 (m, 9H). ^{13}C NMR (126 MHz, DMSO-d6): δ = 179.19 (d, J = 172.6 Hz), 126.88 (d, J = 293.3 Hz), 49.44 - 40.12 (m), 29.07, 17.18 (d, J = 206.6 Hz).

Table S3: GPC results

	Mp	Mw	Mn	Mz	PD
MA-ST-1	10424	10316	8577	12103	1.20
MA-ST-2	12169	11747	10072	13450	1.17
MA-ST-3	12937	12125	9868	14370	1.23
MA-ST-4	13200	12784	10853	14756	1.15
MA-ST-5	14106	11894	8340	15175	1.21
MA-ST-6	15103	13378	10346	16337	1.29
MA-VBA-1	10997	10903	8015	13934	1.36
MA-VBA-2	15514	14381	9964	18685	1.44
AA-ST-1	11273	10858	9185	12403	1.18
AA-ST-2	15132	15515	13172	17736	1.18

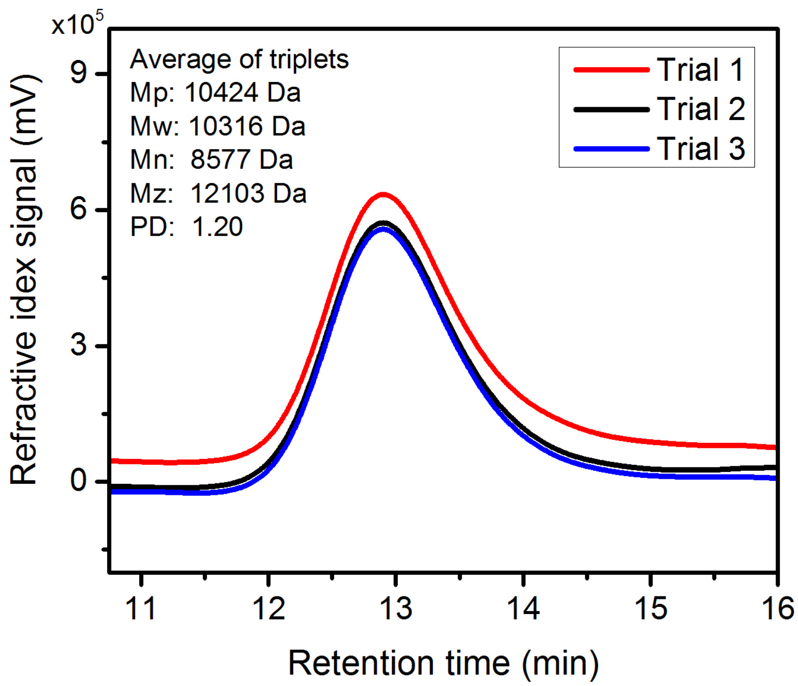

Figure S22: Representative GPC elution curves in characterizing polymer length. The example shown is MA-ST-90. Every polymer has three trials, and the average molecular weights for samples are shown in the table below.

References

(S1) Malde, A. K.; Zuo, L.; Breeze, M.; Stroet, M.; Poger, D.; Nair, P. C.; Oostenbrink, C.; Mark, A. E. An Automated Force Field Topology Builder (ATB) and Repository: Version 1.0. *Journal of Chemical Theory and Computation* **2011**, *7*, 4026–4037.

(S2) Van Der Spoel, D.; Lindahl, E.; Hess, B.; Groenhof, G.; Mark, A. E.; Berendsen, H. J. C. GROMACS: Fast, Flexible, and Free. *Journal of Computational Chemistry* **2005**, *26*, 1701–1718.

(S3) Jorgensen, W. L.; Maxwell, D. S.; Tirado-Rives, J. Development and Testing of the OPLS All-Atom Force Field on Conformational Energetics and Properties of Organic Liquids. *Journal of the American Chemical Society* **1996**, *118*, 11225–11236.

(S4) Jorgensen, W. L.; McDonald, N. A. Development of an All-Atom Force Field for Heterocycles. Properties of Liquid Pyridine and Diazenes. *Journal of Molecular Structure: THEOCHEM* **1998**, *424*, 145–155.

(S5) Kaminski, G. A.; Friesner, R. A.; Tirado-Rives, J.; Jorgensen, W. L. Evaluation and Reparametrization of the OPLS-AA Force Field for Proteins via Comparison with Accurate Quantum Chemical Calculations on Peptides †. *The Journal of Physical Chemistry B* **2001**, *105*, 6474–6487.

(S6) Watkins, E. K.; Jorgensen, W. L. Perfluoroalkanes: Conformational Analysis and Liquid-State Properties from Ab Initio and Monte Carlo Calculations. *The Journal of Physical Chemistry A* **2001**, *105*, 4118–4125.

(S7) Price, M. L. P.; Ostrovsky, D.; Jorgensen, W. L. Gas-Phase and Liquid-State Properties of Esters, Nitriles, and Nitro Compounds with the OPLS-AA Force Field. *Journal of Computational Chemistry* **2001**, *22*, 1340–1352.

(S8) Rizzo, R. C.; Jorgensen, W. L. OPLS All-Atom Model for Amines: Resolution of the Amine Hydration Problem. *Journal of the American Chemical Society* **1999**, *121*, 4827–4836.

(S9) McDonald, N. A.; Jorgensen, W. L. Development of an All-Atom Force Field for Heterocycles. Properties of Liquid Pyrrole, Furan, Diazoles, and Oxazoles. *The Journal of Physical Chemistry B* **1998**, *102*, 8049–8059.

(S10) Schmid, N.; Eichenberger, A. P.; Choutko, A.; Riniker, S.; Winger, M.; Mark, A. E.; van Gunsteren, W. F. Definition and Testing of the GROMOS Force-Field Versions 54A7 and 54B7. *European Biophysics Journal* **2011**, *40*, 843–856.

(S11) Abascal, J. L. F.; Vega, C. A General Purpose Model for the Condensed Phases of Water: TIP4P/2005. *The Journal of Chemical Physics* **2005**, *123*, 234505.

(S12) Bussi, G.; Donadio, D.; Parrinello, M. Canonical Sampling through Velocity Rescaling. *The Journal of Chemical Physics* **2007**, *126*, 014101.

(S13) Parrinello, M.; Rahman, A. Polymorphic Transitions in Single Crystals: A New Molecular Dynamics Method. *Journal of Applied Physics* **1981**, *52*, 7182–7190.

(S14) Nosé, S.; Klein, M. L. Constant Pressure Molecular Dynamics for Molecular Systems. *Molecular Physics* **1983**, *50*, 1055–1076, _eprint: https://doi.org/10.1080/00268978300102851.

(S15) Darden, T.; York, D.; Pedersen, L. Particle Mesh Ewald: An N·log(N) Method for Ewald Sums in Large Systems. *J. Chem. Phys.* **1993**, *98*, 10089–10092.

(S16) Hess, B. P-LINCS: A Parallel Linear Constraint Solver for Molecular Simulation. *J. Chem. Theory Comput.* **2008**, *4*, 116–122.

(S17) Bisker, G.; Dong, J.; Park, H. D.; Iverson, N. M.; Ahn, J.; Nelson, J. T.; Landry, M. P.;

Kruss, S.; Strano, M. S. Protein-Targeted Corona Phase Molecular Recognition. *Nat Commun* **2016**, *7*.

(S18) Choi, J. H.; Strano, M. S. Solvatochromism in Single-Walled Carbon Nanotubes. *Appl. Phys. Lett.* **2007**, *90*, 223114.

(S19) Dielectric Constant. http://polymerdatabase.com/polymer%20physics/Epsilon%20Table.html.